



Modeling Thermodynamic Properties of Mixtures of CO₂ + O₂ in the Allam Cycle by Equations of State

Jens Staubach¹ · Gerhard Schwarz² · Stephan Möbius² · Hans Hasse¹ · Simon Stephan¹

Received: 12 September 2023 / Accepted: 12 November 2023 / Published online: 27 November 2023
© The Author(s) 2023

Abstract

Different equations of state (EOS) were applied for describing thermodynamic properties of the system CO₂ + O₂, which is important for the Allam cycle: cubic EOS (Soave–Redlich–Kwong, Peng–Robinson), molecular-based EOS (PC-SAFT, PCP-SAFT, SAFT-VR Mie, polar soft-SAFT, BACKONE, sCPA), and multiparameter EOS (GERG-2008, EOS-CG). The pure component models were taken from the literature. The results for the mixture were compared to experimental data from the literature for two cases: (i) the thermodynamic properties of the mixture were modeled using predictive mixing and combination rules; (ii) additional binary interaction parameters were fitted to experimental data for improving the performance. In the predictive mode (i), the best results were obtained with molecular-based EOS. In the adjusted mode (ii) the best results were obtained with the multi-parameter GERG-2008 EOS and EOS-CG.

Keywords Allam cycle · Carbon capture · Carbon dioxide · Equation of state · Oxygen

1 Introduction

Power plants based on the Allam cycle generate electric energy as well as CO₂ of high purity at high pressure from burning hydrocarbon fuels with pure oxygen [1]. The process is attractive, as it combines a high thermal efficiency with efficient CO₂ capture [2, 3]. In the simplest picture, the Allam cycle can be described as a

Special Issue in Honor of Professor Roland Span's 60th Birthday.

✉ Simon Stephan
Simon.Stephan@rptu.de

¹ Laboratory of Engineering Thermodynamics (LTD), RPTU Kaiserslautern, 67663 Kaiserslautern, Germany

² KSB SE & Co. KGaA, 67227 Frankenthal, Germany

Joule-Brayton cycle with internal heat recuperation in which the main working fluid is CO_2 . Additionally, oxygen and water are present in the working fluid. Water is removed before the compression and most of the CO_2 is removed after the compression. Hence, for modeling the compression, the knowledge of the properties of mixtures of CO_2 and O_2 is essential. To some extent, also other components can be present such as argon, nitrogen, and trace elements from the fuel. In this work, we focus on the main components CO_2 and O_2 of the working fluid.

For the design of power plants based on the Allam cycle, information on the thermal and caloric properties as well as phase equilibria of the working fluid is needed. The interest in the Allam cycle has led to a number of experimental studies of thermophysical properties of mixtures relevant for the Allam cycle in recent years [4–10] that can be used as basis for the thermodynamic modeling by equations of state (EOS). In principle, EOS can be used to predict mixture properties from pure component properties using predictive mixing and combination rules. Nevertheless, for many applications, such predictions are not accurate enough, so that adjustable binary parameters are introduced that are fitted to selected experimental data of the mixture. In this work, the mixture $\text{CO}_2 + \text{O}_2$ was modeled using different EOS based on pure component models that were taken from the literature. Both, predictive mixing and combination rules as well as mixing and combination rules with adjustable parameters were tested.

Different types of EOS have been used for modeling mixtures of CO_2 with other components, see, e.g. Refs. [4, 11–13]. In 2011, Diamantonis et al. [11] have assessed predictions of cubic EOS and EOS based on statistical association fluid theory (SAFT) for phase equilibria of binary mixtures of CO_2 with (CH_4 , N_2 , O_2 , SO_2 , Ar, and H_2S). The studied EOS included the Redlich–Kwong [14], Soave–Redlich–Kwong (SRK) [15], Peng–Robinson (PR) [16], SAFT [17], and perturbed chain-SAFT (PC-SAFT) [18] EOS. Diamantonis et al. [11] concluded that the PC-SAFT EOS is overall the most accurate EOS for predicting $\text{CO}_2 +$ gas mixture properties. In 2014, Mazzocchi et al. [12] studied different EOS regarding their predictions of phase equilibria and homogeneous state density data of binary mixtures of CO_2 with (N_2 , O_2 , and Ar). The studied EOS included the Benedict–Webb–Rubin (BWR) [19], PC-SAFT, and GERG-2008 [20] EOS. The GERG-2008 and PC-SAFT EOS were found to perform well in most cases. In 2016, Lasala et al. [4] compared different cubic EOS with different combination rules for predicting phase equilibria of binary mixtures of CO_2 with (N_2 , Ar, and O_2) and found that using a temperature-dependent parameter in the combination rule improved the accuracy significantly. In 2017, Perez et al. [13] studied the modeling of vapor–liquid equilibria and homogeneous state densities of 108 binary mixtures related to carbon capture and storage using the SRK, PR, PC-SAFT, and SAFT-VR Mie [21] EOS using a temperature-dependent combination rule parameter. Perez et al. [13] concluded that the SAFT-VR Mie EOS is the most accurate of the studied EOS.

Overall, the findings reported in the literature give no clear picture, which EOS to use for modeling mixture properties of $\text{CO}_2 + \text{O}_2$. Furthermore, a significant amount of new data has become available only recently and was not included in most studies discussed above [4–10]. Therefore, in this work, we have studied the modeling of mixture properties of $\text{CO}_2 + \text{O}_2$ using different EOS. First, the available literature

data are reviewed and compiled in a database. This includes vapor–liquid equilibrium data $Tp x' x''$ as well as homogeneous state property data (density ρ , speed of sound w , and isothermal compressibility β) for a given composition, pressure, and temperature. Ten EOS were used for modeling the mixture properties, namely the SRK [15], PR [16], PC-SAFT [18], PCP-SAFT [18, 22], SAFT-VR Mie [21], polar soft-SAFT [23, 24], BACKONE [25, 26], sCPA [27, 28], GERG-2008 [20], and EOS-CG [29] EOS. The EOS-CG as well as pure component EOS models for CO_2 and O_2 [30, 31] were developed by Roland Span and co-workers.

Two cases were considered: (i) the thermodynamic properties of the mixture were modeled using fully predictive mixing and combination rules (“predictive mode”); (ii) temperature-dependent binary interaction parameters were fitted to a training dataset of experimental data for improving the performance of the models (“adjusted mode”). The binary interaction parameters were fitted to the same training dataset for all studied EOS; except the EOS-CG [29]. The binary interaction parameters for the mixture $\text{CO}_2 + \text{O}_2$ were already fitted in the original publication by Gernert and Span [29] and they are adopted here for the EOS-CG in the “adjusted mode”. The results are compared for both cases (i) and (ii) for the complete literature data, a training, and a test dataset. This allows a comparison of the different EOS on an equal basis.

This paper is structured as follows: first, the experimental data basis for mixtures of $\text{CO}_2 + \text{O}_2$ that was established from literature data is presented; then, the studied EOS are described, focusing in the modeling of mixture properties. Finally, the results of the application of the EOS in the predictive and adjusted mode are presented and critically compared.

2 Methods

2.1 Experimental Data Basis

Tables 1 and 2 give an overview of the available experimental data on the vapor–liquid equilibrium and homogeneous state property data, respectively, in the system $\text{CO}_2 + \text{O}_2$. In total, 255 phase equilibrium data points and 1866 homogeneous state data points have been reported. The phase equilibrium datasets report pressure p and the compositions of both phases x' , x'' for a given temperature T . For the homogeneous states, data on the density ρ , the speed of sound w , and the isothermal compressibility β at a given pressure and temperature are available. The database compiled within this work is provided in the electronic Supplementary Information.

Phase equilibrium data (cf. Table 1) have been reported in the literature in the range $218 \text{ K} \leq T \leq 298 \text{ K}$, $0.9 \text{ MPa} \leq p \leq 14.4 \text{ MPa}$, and $0.0 \text{ mol}\cdot\text{mol}^{-1} < x_{\text{O}_2} \leq 0.55 \text{ mol}\cdot\text{mol}^{-1}$. The phase equilibrium data covers almost the complete range between the temperature of the triple point and the critical temperature of pure CO_2 ($T_{\text{tr,CO}_2} = 216.58 \text{ K}$ [32, 33], $T_{\text{c,CO}_2} = 304.15 \text{ K}$ [34]). The data on homogeneous state points lie in the region $250 \text{ K} \leq T \leq 423 \text{ K}$, $0.5 \text{ MPa} \leq p \leq 47.8 \text{ MPa}$, and $0.0 \text{ mol}\cdot\text{mol}^{-1} < x_{\text{O}_2} \leq 0.75 \text{ mol}\cdot\text{mol}^{-1}$. The critical temperature of oxygen is

Table 1 Overview of studies reporting experimental data on vapor–liquid equilibrium properties of the system CO₂ + O₂

References	Year	<i>N</i>	Ranges		
			<i>T</i> / K	<i>p</i> / MPa	<i>x</i> ' _{O₂} / mol · mol ⁻¹
Lasala et al. [4, 5]	2016	67	223–293	1.7–13.9	0.01–0.45
Westman et al. [6]	2016	61	218–298	2.0–14.4	0.01–0.55
Ahmad et al. [61]	2014	11	277–298	4.1–8.1	0.02–0.05
Fredenslund et al. [62]	1972	11	224	0.9–14.2	0.01–0.45
Fredenslund and Sather [63]	1970	71	223–283	1.0–13.2	0.01–0.39
Kaminishi et al. [64]	1966	16	233–298	3.7–12.7	0.03–0.37
Chueh et al. [65]	1965	4	273	5.5–11.7	0.05–0.31
Zenner and Dana [66]	1963	25	218–273	2.2–14.3	0.03–0.50

N is the number of data points

The last three columns give information on the range of states in which data are provided: *T* and *p* are temperature and pressure, *x*'_{O₂} is the liquid phase mole fraction of O₂

Table 2 Overview of studies reporting experimental data on homogeneous state point properties of the system CO₂ + O₂

References	Year	<i>N</i>	Ranges		
			<i>T</i> / K	<i>p</i> / MPa	<i>x</i> _{O₂} / mol · mol ⁻¹
<i>ppT</i>					
Lozano-Martin et al. [8]	2021	274	250–375	0.5–19.8	0.50–0.75
Ahamada et al. [10]	2020	820	277–416	1.0–20.5	0.13–0.48
Lozano-Martin et al. [7]	2020	162	250–375	0.5–13.1	0.05–0.20
Commodore et al. [9]	2018	112	324–400	2.3–35.3	0.01
Al-Siyabi [67]	2013	72	283–423	7.7–47.8	0.05
Mantovani et al. [34]	2012	196	303–383	1.0–20.0	0.06–0.13
Mazzocoli et al. [68]	2012	106	273–293	1.0–20.0	0.04–0.15
Gururaja et al. [69]	1967	7	297–298	1.3–1.6	0.08–0.81
<i>w, β</i>					
Al-Siyabi [67]	2013	62	268–301	8.9–41.0	0.07

N is the number of data points

The last three columns give information on the range of states in which data are provided: *T* and *p* are temperature and pressure, *x*_{O₂} is the mole fraction of O₂

*T*_{c,O₂} = 154.77 K [34]. Hence, oxygen is supercritical in the entire studied temperature range. The mixture CO₂ + O₂ is a type I mixture according to the scheme of van Konynenburg and Scott [35].

The literature data were checked for clear outliers by comparison of each data point to the rest of the data along isotherms and isobars at equal compositions. Overall, seven data points for VLE and 12 data

Table 3 Number of experimental data for homogeneous state point properties and vapor–liquid equilibrium properties of the system CO₂ + O₂ used in the comparison of the EOS

Property Region	N_ρ			N_β	N_w	$N_{x'}$	$N_{x''}$
	Liquid	Supercritical	Vapor	Supercritical	Supercritical		
All data	41	1371	325	62	62	259	259
Training data	41	391	105	32	32	91	89
Test data	0	980	220	30	30	168	170

The number of data points N is reported for the density ρ , isothermal compressibility β , speed of sound w , liquid phase composition x' and vapor phase composition x''

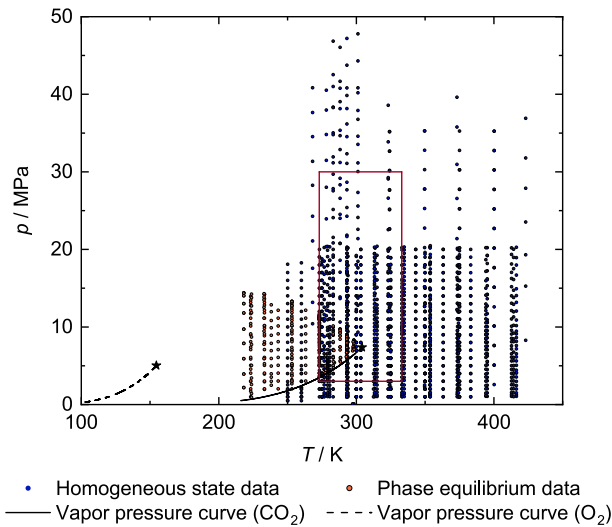


Fig. 1 Pressure–temperature diagram with the homogeneous state data and phase equilibrium data compiled in the database, cf. Tables 1 and 2. Additionally, the vapor pressure curves of CO₂ and O₂ are shown (computed from the reference EOS models from Refs. [30, 43]). The star indicates the critical points. The area of the training data are marked by the red box (Color figure online)

points for homogeneous state points were removed for the EOS evaluation; for details see Supplementary Information. The remaining experimental data were split into a training dataset and a test dataset. The training dataset comprises of data between $273 \text{ K} \leq T \leq 333 \text{ K}$, $5 \text{ MPa} \leq p \leq 30 \text{ MPa}$, and $0.0 \text{ mol}\cdot\text{mol}^{-1} < x_{\text{O}_2} \leq 0.5 \text{ mol}\cdot\text{mol}^{-1}$. The test dataset includes the remaining data. An overview of the number of experimental data points in each dataset is given in Table 3. Additionally, Fig. 1 gives an overview of the temperatures and pressures for which data are available.

Table 4 Overview of the equation of states (EOS) used in this work including information on the basic publication of the EOS and its year, and the publications from which the pure component models were taken together with the number of parameters (indicated by #)

EOS	Year	Reference		
		EOS	CO ₂	O ₂
Cubic				
SRK	1972	[15]	[34] #3	[34] #3
PR	1976	[16]	[34] #3	[34] #3
Molecular-based				
PC-SAFT	2001	[18]	[39] #3	[39] #3
PCP-SAFT	2005	[18, 22]	[22] #4	[39] #3
SAFT-VR Mie	2013	[21]	[38] #4	[38] #4
polar soft-SAFT	2020	[23, 24]	[37] #5	[36] #3
BACKONE	1996	[25, 26]	[25] #4	[25] #3
sCPA	1999	[27, 28]	[40] #5	[41] #3
Multi-parameter				
GERG-2008	2012	[20]	[42] #22	[31] #12
EOS-CG	2016	[29]	[30] #42	[43] #32

2.2 Equations of State

In this work, ten EOS were used for the modeling of mixture properties for the system CO₂ + O₂. Table 4 gives an overview of the EOS used in this work. For all calculations carried out in this work, an in-house code was used that was validated by comparing the results with data from the EOS developers.

All EOS were implemented using the Helmholtz energy formulation. The Helmholtz energy per particle $a = A/N$ can be written as a sum of the ideal gas contribution and a configurational contribution as

$$\frac{a}{k_{\text{B}}T} = \tilde{a} = \tilde{a}_{\text{id}} + \tilde{a}_{\text{config}}. \quad (1)$$

The configurational contribution $\tilde{a}_{\text{config}}$ is calculated by the respective EOS. For the ideal gas contribution \tilde{a}_{id} , the pure component models from Kunz and Wagner [20] were used in all cases. The ideal gas contribution of the total Helmholtz energy of a mixture is calculated as

$$\tilde{a}_{\text{id}} = \sum_{i=1}^N x_i [\tilde{a}_{\text{id},i}(\rho, T) + \ln x_i], \quad (2)$$

where $\tilde{a}_{\text{id},i}$ is the ideal gas contribution of the pure components $i = \text{CO}_2$ and O₂ and x_i indicates the mole fraction of component i . The pure component EOS models for CO₂ and O₂ were taken from the literature in all cases. In all cases, VLE data were used for their parametrization [20, 22, 25, 34, 36–41]—in some cases, additionally, homogeneous state property data were used [20, 22]. The pure component model parameters are summarized in the Supplementary Material.

2.2.1 Multi-parameter EOS

The GERG-2008 [20] EOS and the EOS-CG [29] are empirical multi-parameter EOS. The pure component parameters have no direct physical meaning. They are substance-specific and were correlated in the original works [30, 31, 42, 43] to a large number of experimental data for the respective substance. This leads to very accurate models for the pure substances regarding the data that was used for the fitting. Yet, using multi-parameter EOS for extrapolation, i.e. outside the state range that was considered for the model parametrization, has to be done with caution [44–48]. The two multi-parameter EOS models used here for describing the mixture CO₂ + O₂ use different pure component models, cf. Table 4. The GERG-2008 EOS uses the pure component EOS models from Refs. [31, 42], whereas the EOS-CG uses those from Refs. [30, 43].

For multi-parameter EOS, the extension to mixtures is usually carried out by defining a reducing function for the mixture density $\rho_r(x)$ and mixture temperature $T_r(x)$. Thereby, the configurational contribution to the Helmholtz energy of the mixture can be written as

$$\tilde{a}_{\text{config}}^{\text{multi-parameter}} = \tilde{a}_{\text{config}}\left(\frac{\rho}{\rho_r}, \frac{T_r}{T}, x\right). \tag{3}$$

The reducing functions are calculated according to Ref. [20] as

$$\frac{1}{\rho_r} = \sum_{i=1}^N \sum_{j=1}^N x_i x_j \beta_{v,ij} \gamma_{v,ij} \cdot \frac{x_i + x_j}{\beta_{v,ij}^2 x_i + x_j} \cdot \frac{1}{8} \left(\frac{1}{\rho_{c,i}^{1/3}} + \frac{1}{\rho_{c,j}^{1/3}} \right)^3, \tag{4}$$

and

$$T_r = \sum_{i=1}^N \sum_{j=1}^N x_i x_j \beta_{T,ij} \gamma_{T,ij} \cdot \frac{x_i + x_j}{\beta_{T,ij}^2 x_i + x_j} \cdot (T_{c,i} T_{c,j})^{0.5}, \tag{5}$$

with the critical temperature $T_{c,i}$, $T_{c,j}$ and critical density $\rho_{c,i}$, $\rho_{c,j}$ of component i and j . Both, the GERG-2008 EOS and the EOS-CG use the mixture ansatz outlined in Eqs. 3–5. The parameters ($\beta_{v,ij}$, $\beta_{T,ij}$, $\gamma_{v,ij}$, $\gamma_{T,ij}$) are adjustable mixture parameters in the GERG-2008 and EOS-CG model. They obey the relations [20]

$$\beta_{v,ij} = 1/\beta_{v,ji}, \quad \beta_{T,ij} = 1/\beta_{T,ji}, \tag{6}$$

and

$$\gamma_{v,ij} = \gamma_{v,ji}, \quad \gamma_{T,ij} = \gamma_{T,ji}. \tag{7}$$

An additional departure function can be regressed to mixture properties for multi-parameter EOS to improve their accuracy [20, 49] which was, however, not used here.

2.2.2 Cubic EOS

The SRK [15] and PR [16] EOS were implemented according to Ref. [50] in the Helmholtz energy form. The pure component models are specified by the numbers for the critical temperature T_c , the critical pressure p_c , and the acentric factor ω . The corresponding numbers are given in the Supplementary Information. The standard one-fluid mixing rules were applied for the calculation of the mixture attraction energy parameter a_m and the mixture co-volume parameter b_m :

$$a_m = \sum_{i=1}^N \sum_{j=1}^N x_i x_j a_{ij}(T), \quad (8)$$

$$b_m = \sum_{i=1}^N \sum_{j=1}^N x_i x_j b_{ij}. \quad (9)$$

For the calculation of the cross-interaction parameters between the components i and j , the modified Lorentz-Berthelot combination rules were used, i.e.

$$a_{ij}(T) = \xi_{ij} \sqrt{a_{ii}(T) a_{jj}(T)}, \quad (10)$$

and

$$b_{ij} = \frac{1}{2}(b_{ii} + b_{jj}), \quad (11)$$

where ξ_{ij} is a binary interaction parameter.

2.2.3 Molecular-based EOS

Six molecular-based EOS were used in this work: PC-SAFT [18], PCP-SAFT [18, 22], SAFT-VR Mie [21], polar soft-SAFT [23, 24], BACKONE [25, 26], and sCPA [27, 28] EOS. In these EOS the different molecular features are represented by independent terms in the Helmholtz energy. The configurational Helmholtz energy is formulated as

$$\tilde{a}_{\text{config}} = \tilde{a}_{\text{rep}} + \tilde{a}_{\text{disp}} + \tilde{a}_{\text{chain}} + \tilde{a}_{\text{polar}} + \tilde{a}_{\text{assoc}}, \quad (12)$$

with the repulsion \tilde{a}_{rep} , dispersion \tilde{a}_{disp} , chain \tilde{a}_{chain} , polar \tilde{a}_{polar} , and association \tilde{a}_{assoc} contribution. Table 5 gives an overview of the terms used in the different molecular-based EOS. For O_2 , the basic modeling approach was the same for all EOS, i.e. dispersive and repulsive interactions as well as the molecule elongation are modeled. For CO_2 , in addition to these terms, in some cases, the polarity of the molecule was explicitly described by an additional term. Different approaches are used for this in the EOS shown in Table 5: a polar term is used for the PCP-SAFT, polar soft-SAFT and BACKONE and an association term in the sCPA.

Table 5 Overview of the configurational Helmholtz energy terms used in the modeling of CO₂ and O₂ for each of the studied molecular-based EOS models

EOS	Substance	Repulsion	Dispersion	Chain (elongation)	Polar	Association
PC-SAFT	O ₂	X	X	X		
	CO ₂	X	X	X		
PCP-SAFT	O ₂	X	X	X		
	CO ₂	X	X	X	X	
SAFT-VR Mie	O ₂	X	X	X		
	CO ₂	X	X	X		
Polar soft-SAFT	O ₂	X	X	X		
	CO ₂	X	X	X	X	
BACKONE	O ₂	X	X	X		
	CO ₂	X	X	X	X	
sCPA	O ₂	X	X	X		
	CO ₂	X	X	X		X

The pure component model parameters were taken from the literature

The pure component models used for the PC-SAFT [18], PCP-SAFT [18, 22], SAFT-VR Mie [21], and polar soft-SAFT [23, 24] have (at least) three parameters: the size parameter σ , dispersion energy parameter ϵ , and the chain length parameter m . The SAFT-VR Mie [21] models have an additional adjustable parameter λ_r , which indicates the repulsion exponent for the Mie potential [51]. Moreover, the quadrupole terms of the PCP-SAFT and polar soft-SAFT have the quadrupole moment as an additional parameter. The quadrupole term used in the polar soft-SAFT EOS has an additional parameter x_p , which describes the number of quadrupole elements in the molecule (modeling the delocalization of the quadrupole). The BACKONE [25, 26] EOS incorporates the parameter α (instead of the chain length parameter m) modeling the elongation of the molecule. The sCPA [27, 28] EOS combines the Helmholtz energy term from the SRK EOS \tilde{a}^{SRK} for modeling dispersive and repulsive interactions with an association term \tilde{a}_{assoc} . Since CO₂ is modeled with the association term, it has two additional parameters: the association energy parameter $\hat{\epsilon}$ and the association volume parameter $\hat{\beta}$. Details and the numeric values of the parameters of the pure component models, that were taken from the literature [22, 24, 25, 36, 38–41], are given in the Supplementary Information.

The mixing rules used in the molecular-based EOS were directly adopted from the original works [18, 21–28]. In the sCPA EOS, the cross-interaction parameters between the components were computed according to Eqs. 8–11 (see above). For the PC-SAFT, the PCP-SAFT, polar soft-SAFT, and the BACKONE EOS, the modified Lorentz-Berthelot combination rules were used, i.e.

$$\epsilon_{ij} = \xi_{ij} \sqrt{\epsilon_{ii} \epsilon_{jj}}, \quad (13)$$

$$\sigma_{ij} = \frac{1}{2}(\sigma_{ii} + \sigma_{jj}). \quad (14)$$

In the SAFT-VR Mie EOS, the energy cross-interaction parameter was computed with the combination rule

$$\varepsilon_{ij} = \xi_{ij} \frac{\sqrt{\sigma_{ii}^3 \sigma_{jj}^3}}{\sigma_{ij}^3} \sqrt{\varepsilon_{ii} \varepsilon_{jj}}, \quad (15)$$

while σ_{ij} was calculated according to Eq. 14. Therein, the binary interaction parameter ξ_{ij} is treated the same as the binary interaction parameter of the cubic EOS, cf. Eq. 10. For the chain term, polar term, and association term, no combination rule applies.

2.2.4 Regression of Binary Interaction Parameters

First, all EOS were used in a purely predictive mode, i.e. no mixture parameters were adjusted. In the *predictive mode*, we have used the multi-parameter EOS with $\beta_{v,\text{CO}_2,\text{O}_2} = \beta_{T,\text{CO}_2,\text{O}_2} = \gamma_{v,\text{CO}_2,\text{O}_2} = \gamma_{T,\text{CO}_2,\text{O}_2} = 1$, cf. Eqs. 4 and 5. The cubic and molecular-based EOS were used in the predictive mode with $\xi_{\text{CO}_2,\text{O}_2} = 1$, cf. Eqs. 10, 13, and 15. For the multi-parameter EOS, in the predictive mode, the Lorentz–Berthelot combination rules were applied. For the GERG-2008 EOS, the predictive mode corresponds to the EOS model as originally proposed by Kunz and Wagner [20], which was not adjusted to $\text{CO}_2 + \text{O}_2$ mixture data. For the EOS-CG, the predictive mode reflects a simplified version of the original EOS-CG model that was fitted to $\text{CO}_2 + \text{O}_2$ mixture data by Gernert and Span [29].

Additionally, the binary interaction parameters were regressed to the training set of the mixture data in an *adjusted mode*. The obtained models were compared to the predictive mode models. For the cubic and molecular-based EOS, the cross-interaction energy parameter $\xi_{\text{CO}_2,\text{O}_2}$ was adjusted. Therefore, a linear temperature-dependent function was used

$$\xi_{\text{CO}_2,\text{O}_2} = o_1 + o_2 \cdot (T/\text{K}), \quad (16)$$

where o_1 and o_2 are the adjustable parameters. For the GERG-2008 EOS, the four binary interaction parameters $\bar{o} = \beta_{v,\text{CO}_2,\text{O}_2}, \beta_{T,\text{CO}_2,\text{O}_2}, \gamma_{v,\text{CO}_2,\text{O}_2}, \gamma_{T,\text{CO}_2,\text{O}_2}$ were adjusted. For the EOS-CG, the binary interaction parameters $\gamma_{v,\text{CO}_2,\text{O}_2}, \gamma_{T,\text{CO}_2,\text{O}_2}$ were adapted for the adjusted mode from the original work by Gernert and Span [29] with $\beta_{v,\text{CO}_2,\text{O}_2}, \beta_{T,\text{CO}_2,\text{O}_2} = 1$. Hence, for the cubic, molecular-based EOS, and the EOS-CG two adjustable parameters were used, whereas four adjustable parameters were used for the GERG-2008 EOS. This follows the usual way these model classes are used for mixture modeling [20, 29, 49, 52–55].

The binary interaction parameters \bar{o}^k for the EOS k were obtained by minimizing a least-squares objective function F given by

Table 6 Binary interaction parameters for the mixture CO₂ + O₂ obtained from the regression to experimental data, cf. Eq. 16

EOS	o_1	o_2
SRK	0.2970 469	2.3560 240 × 10 ⁻³
PR	1.1025 889	- 7.3000 922 × 10 ⁻⁴
PC-SAFT	1.0819 439	- 4.6704 942 × 10 ⁻⁴
PCP-SAFT	1.3391 420	- 1.1561 565 × 10 ⁻³
SAFT-VR Mie	1.0749 257	- 2.2777 264 × 10 ⁻⁴
polar soft-SAFT	1.2515 353	- 8.9082 688 × 10 ⁻⁴
BACKONE	1.3151 601	- 1.1994 463 × 10 ⁻³
sCPA	1.2425 680	- 9.0735 012 × 10 ⁻⁴

Table 7 Binary interaction parameters for the mixture CO₂ + O₂ obtained from the regression to experimental data for the GERG-2008 EOS, cf. Eqs. 4 and 5

EOS	β_{v,CO_2,O_2}	β_{T,CO_2,O_2}	γ_{v,CO_2,O_2}	γ_{T,CO_2,O_2}
GERG-2008	0.976180 838	1.011636 925	1.213083 507	1.008384 202

$$\begin{aligned}
 \min_{\vec{\sigma}^k} F(\vec{\sigma}^k) = & \frac{1}{N_\rho} \sum_{t=1}^{N_\rho} \left[\frac{\rho_t^{EOS} - \rho_t^{Ref}}{\rho_t^{Ref}} \right]^2 + \frac{1}{100 \cdot N_\beta} \sum_{t=1}^{N_\beta} \left[\frac{\beta_t^{EOS} - \beta_t^{Ref}}{\beta_t^{Ref}} \right]^2 \\
 & + \frac{1}{10 \cdot N_w} \sum_{t=1}^{N_w} \left[\frac{w_t^{EOS} - w_t^{Ref}}{w_t^{Ref}} \right]^2 + \frac{0.5}{N_{x'_{O_2}}} \sum_{t=1}^{N_{x'_{O_2}}} \left[x'_{O_2,t}{}^{EOS} - x'_{O_2,t}{}^{Ref} \right]^2 \quad (17) \\
 & + \frac{0.5}{N_{x''_{O_2}}} \sum_{t=1}^{N_{x''_{O_2}}} \left[x''_{O_2,t}{}^{EOS} - x''_{O_2,t}{}^{Ref} \right]^2
 \end{aligned}$$

where the superscript Ref indicates the experimental data points and the superscript EOS indicates the value computed by a given EOS and N_l indicates the number of data points for the properties $l = \rho, \beta, w, x'_{O_2}$, and x''_{O_2} . Only experimental data from the training set were considered in the fitting procedure, cf. Fig. 1. The weights used in the fit, cf. Eq. 17, were determined in an iterative approach such that a good compromise between the individual objectives was obtained. The isothermal compressibility data and speed of sound data were weighted considerably less (1/100 and 1/10 times less, respectively) compared to the homogeneous state density data since they were only available for a single composition of the mixture ($x_{O_2} = 0.0652 \text{ mol} \cdot \text{mol}^{-1}$).

The adjusted parameters o_1 and o_2 for the cubic and molecular-based EOS are given in Table 6. The adjusted binary interaction parameters for the GERG-2008 [20] EOS $\beta_{v,CO_2,O_2}, \beta_{T,CO_2,O_2}, \gamma_{v,CO_2,O_2}, \gamma_{T,CO_2,O_2}$ are given in Table 7. Note, that the

mixture parameters for the EOS-CG as proposed in Ref. [29] were obtained by regression to a wider temperature range compared to the training dataset used in this work.

2.2.5 Assessment of the EOS

The performance of the different EOS used in both the predictive and adjusted mode was evaluated in a systematic way. For all EOS, the performance for the homogeneous state properties and the phase equilibrium properties was evaluated. Therefore, mean deviations from a given model and the experimental data were computed. For the homogeneous state properties, the mean absolute relative deviation $\delta_{lm}^{\text{rel},k}$ was calculated for each of the studied EOS k for the properties $l = \rho, \beta$, and w for the fluid region $m = \text{vapor, liquid, and supercritical by}$

$$\delta_{lm}^{\text{rel},k} = \frac{1}{N_{lm}} \sum_{i=1}^{N_{lm}} \left| 100 \% \frac{Y_{lm}^{\text{EOS}} - Y_{lm}^{\text{Ref}}}{Y_{lm}^{\text{Ref}}} \right|, \quad (18)$$

where Y^{Ref} indicates the value of the experimental data point taken from the literature. For the homogeneous state point properties, the assignment of the data points from the literature to the fluid regions was carried out by estimating the critical temperatures depending on the composition from the experimental phase boundary data (see electronic Supplementary Information). The mean absolute relative deviation $\delta_{lm}^{\text{rel},k}$ is therefore a measure for the performance of the EOS k for the property l in the fluid region m .

The performance of the EOS models for describing the vapor–liquid equilibrium phase boundary was evaluated by the mean absolute deviation $\delta_n^{\text{abs},k}$ for phase composition for a given temperature and pressure defined as

$$\delta_n^{\text{abs},k} = \frac{1}{N_n} \sum_{i=1}^{N_n} |x_{\text{O}_2,ni}^{\text{EOS}} - x_{\text{O}_2,ni}^{\text{Ref}}|, \quad (19)$$

where n represents the liquid ($n = \text{liq}$) and vapor ($n = \text{vap}$) side of the phase boundary.

Both mean deviations $\delta_{lm}^{\text{rel},k}$ and $\delta_n^{\text{abs},k}$ were calculated for three cases: (i) for all data points available for the mixture $\text{CO}_2 + \text{O}_2$, (ii) for the data points considered for the mixture parametrization, i.e. the training data (cf. Fig. 1), and (iii) the test data.

3 Results and Discussion

3.1 Vapor–Liquid Equilibrium

The results for the mean absolute deviation in the liquid and vapor phase mole fraction $\delta_{\text{liq}}^{\text{abs}}$ and $\delta_{\text{vap}}^{\text{abs}}$, respectively, are given in Table 8. Additionally, Fig. 2 shows the

Table 8 Overview of the quality of the description of experimental VLE data for the system $\text{CO}_2 + \text{O}_2$ by different EOS. Results from predictions based on pure component models are compared to results that were obtained after adjusting binary parameters (given in brackets) to the training data. Results are reported for each EOS from top to bottom for all data, the training data, and the test data. For details, see text

EOS	No phase split	$\delta_{\text{liq}}^{\text{abs}}$ / mol · mol ⁻¹	$\delta_{\text{vap}}^{\text{abs}}$ / mol · mol ⁻¹
PR	28 (0)	0.075 (0.025)	0.018 (0.022)
	9 (0)	0.044 (0.009)	0.020 (0.023)
	19 (0)	0.092 (0.034)	0.017 (0.022)
SRK	21 (0)	0.071 (0.040)	0.020 (0.032)
	3 (0)	0.042 (0.024)	0.024 (0.026)
	18 (0)	0.088 (0.048)	0.018 (0.035)
PC-SAFT	3 (0)	0.051 (0.024)	0.026 (0.026)
	0 (0)	0.020 (0.012)	0.036 (0.030)
	3 (0)	0.069 (0.031)	0.021 (0.024)
PCP-SAFT	0 (2)	0.035 (0.036)	0.029 (0.025)
	0 (0)	0.019 (0.011)	0.024 (0.024)
	0 (2)	0.044 (0.050)	0.031 (0.025)
SAFT-VR Mie	0 (0)	0.028 (0.024)	0.019 (0.018)
	0 (0)	0.026 (0.020)	0.019 (0.019)
	0 (0)	0.029 (0.026)	0.019 (0.018)
polar soft-SAFT	0 (0)	0.042 (0.026)	0.050 (0.045)
	0 (0)	0.027 (0.025)	0.063 (0.063)
	0 (0)	0.050 (0.027)	0.043 (0.036)
BACKONE	0 (0)	0.041 (0.033)	0.065 (0.063)
	0 (0)	0.021 (0.024)	0.078 (0.076)
	0 (0)	0.051 (0.037)	0.058 (0.056)
sCPA	0 (0)	0.018 (0.030)	0.044 (0.043)
	0 (0)	0.011 (0.012)	0.053 (0.053)
	0 (0)	0.023 (0.040)	0.039 (0.037)
GERG-2008	0 (26)	0.069 (0.017)	0.039 (0.016)
	0 (0)	0.038 (0.007)	0.048 (0.017)
	0 (26)	0.085 (0.024)	0.035 (0.015)
EOS-CG	0 (11)	0.069 (0.014)	0.039 (0.026)
	0 (0)	0.038 (0.008)	0.047 (0.036)
	0 (11)	0.085 (0.017)	0.035 (0.020)

phase envelopes obtained from the EOS in comparison with experimental data for three different temperatures. Both, Table 8 and Fig. 2 show the results for the predictive mode and the adjusted mode.

The critical pressure obtained from the predictive calculations by most studied EOS significantly overestimates the highest pressures reported by the experimental data for the studied temperatures, cf. Fig. 2. The only exceptions are the PR and SRK EOS, which in return yield high deviations for the liquid phase composition, cf. Table 8. A good prediction of the studied phase envelopes (top row in Fig. 2) is obtained for the SAFT-VR Mie and the PCP-SAFT EOS, which is also reflected in the mean deviations given in Table 8. The inclusion of the quadrupole in the model

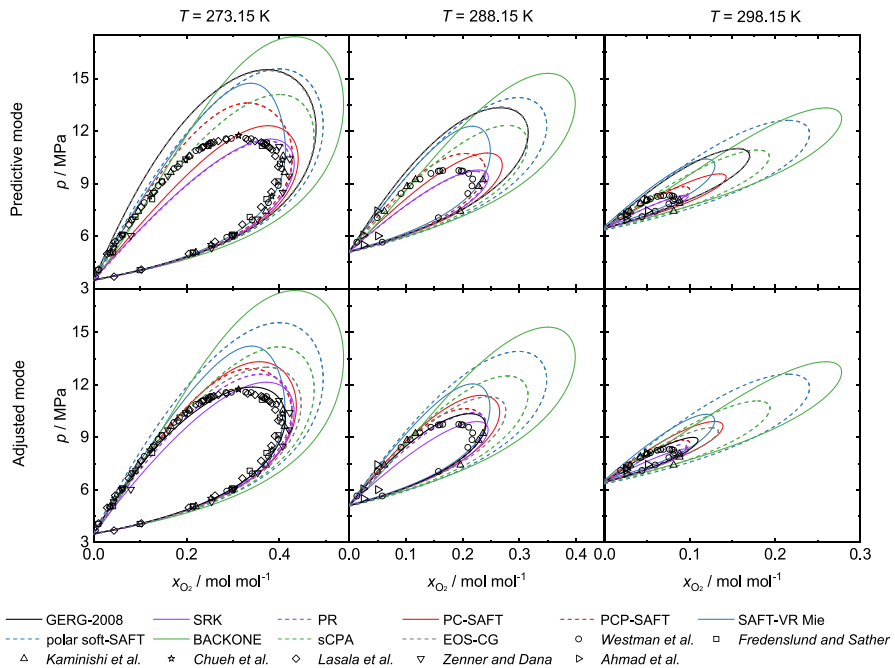


Fig. 2 Phase envelope of the system $\text{CO}_2 + \text{O}_2$ calculated by different EOS (lines) compared to literature data (symbols) [4, 6, 61, 63–66]. Results from predictions based on pure component models (top) are compared to results that were obtained after adjusting binary parameters (bottom) to the training data. The GERG-2008 and EOS-CG results collapse to one line in the top figures (predictive mode). For details, see text (Color figure online)

of CO_2 of the PCP-SAFT EOS compared to the PC-SAFT model reduces the deviations in the liquid phase composition and overall improves the description of the phase boundary for the temperatures $T / \text{K} = 288.15, 298.15$, cf. Fig. 2. The multi-parameter GERG-2008 EOS yields high deviations for the liquid side composition $\delta_{\text{liq}}^{\text{abs}}$ and also significantly overestimates the critical point. The EOS-CG yields almost identical results for the predictive calculations as the GERG-2008 EOS. This is interesting, since different pure component models are used in the GERG-2008 EOS and EOS-CG.

For the adjusted mode, the performance of all models significantly improves for the training dataset—as expected. In particular, the results obtained from the adjusted GERG-2008 EOS are in very good agreement with the experimental data. One reason for this may be that four parameters were used for the adjustment. The PR EOS also yields significantly lower deviations compared to the predictive mode and is on a par with the adjusted GERG-2008 EOS with only two parameters. For the liquid phase concentration deviations, the EOS-CG and the adjusted GERG-2008 EOS yield practically identical results (especially for the training dataset). On the contrary, for the vapor phase, the adjusted GERG-2008 EOS yields significantly lower concentration deviations compared to the EOS-CG, cf. Table 8. For

the molecular-based EOS, the SAFT-VR Mie and the PCP-SAFT EOS yield a good description of the phase envelope in the adjusted mode (only two adjusted parameters). Both EOS overestimate the critical point, but the SAFT-VR Mie EOS overestimates the critical point stronger compared to the PCP-SAFT EOS, cf. Fig. 2. A more detailed discussion on the overestimation of the critical point by the molecular-based EOS is given in the Supplementary Information. Interestingly, the description of the phase envelope by the polar soft-SAFT, BACKONE, and sCPA show almost no improvement by the adjustment of the binary interaction parameters. For the sCPA, this could be the result of modeling CO₂ as an associating fluid. The association contribution is not influenced by the binary interaction parameter since only CO₂ exhibits associating sites in the mixture.

The models (both predictive mode and adjusted mode) were also tested for describing the phase behavior at low temperatures, i.e. for the test dataset. The parameter adjustment also improves the performance of the PR, SRK, and PC-SAFT for the test data liquid phase composition significantly. On the other hand, the mean deviations for the vapor phase composition $\delta_{\text{vap}}^{\text{abs}}$ increase only slightly. The temperature-dependent binary interaction parameter also results in an improvement in the description of the phase envelope at lower temperatures for the more complex models PCP-SAFT and SAFT-VR Mie. For the adjusted GERG-2008 EOS, some deviations occur for the phase equilibria at $T \approx 240$ K. This is not surprising considering the empirical character of the GERG-2008 model type. The EOS-CG on the other hand, yields low deviations even for $T \approx 240$ K, which is probably due to the fact that the mixture model parameters were adjusted to a wider temperature range [29]. Adjusting the mixture parameters of the GERG-2008 model to a wider temperature range most likely would improve the model performance.

3.2 Homogeneous State Properties

The mean average relative deviation δ^{rel} results for homogeneous state properties are reported in Table 9. Additionally, deviation plots for the homogeneous state densities are given in the Supplementary Information. In the predictive mode, i.e. not using adjusted mixture parameters, the GERG-2008 EOS and (simplified) EOS-CG yield overall the best results, especially for the speed of sound and the liquid density. The molecular-based PCP-SAFT and SAFT-VR Mie EOS also yield low deviations for the density. For most molecular-based and both cubic EOS, relatively large deviations are obtained for the 2nd-order derivative properties (isothermal compressibility β and speed of sound w). This is in line with results reported in the literature [56–59] and probably due to the fact that the pure component models were in most cases not adjusted to homogeneous state property data. The isothermal compressibility β is predicted with mean deviations of approximately 5% by the PC-SAFT EOS. Interestingly, the PCP-SAFT EOS, which uses additionally a quadrupole contribution for CO₂, yields lower deviations for the density, but almost equivalent mean deviations for the 2nd-order derivative properties (isothermal compressibility β and speed of sound w) compared to the PC-SAFT EOS. This is likely a result of different fitting strategies used for the development of the pure component models [22, 60].

Table 9 Overview of the quality of the description of experimental homogeneous state data for the system CO₂ + O₂ by different EOS

EOS	Property Region	ρ			β		w
		Liquid	Supercritical	Vapor	Supercritical	Supercritical	
PR		3.11 (2.42)	3.37 (1.93)	3.20 (2.11)	28.33 (32.55)	13.51 (14.35)	
		3.11 (2.42)	5.38 (2.45)	5.82 (3.69)	32.83 (38.39)	11.97 (12.99)	
		–	2.57 (1.73)	1.95 (1.36)	23.53 (26.33)	15.15 (15.80)	
SRK		8.73 (9.28)	2.95 (2.76)	1.60 (1.42)	30.06 (31.06)	10.84 (11.06)	
		8.73 (9.28)	4.60 (4.46)	3.18 (2.76)	33.44 (34.44)	9.00 (9.20)	
		–	2.29 (2.08)	0.84 (0.78)	26.46 (27.47)	12.81 (13.04)	
PC-SAFT		1.72 (1.01)	2.95 (1.68)	2.40 (1.91)	4.42 (4.29)	4.98 (4.03)	
		1.72 (1.01)	4.57 (2.08)	4.50 (3.67)	4.95 (4.76)	7.96 (6.62)	
		–	2.30 (1.52)	1.39 (1.06)	3.87 (3.79)	1.81 (1.26)	
PCP-SAFT		1.38 (1.79)	1.90 (1.62)	1.58 (1.72)	5.96 (6.53)	5.95 (6.11)	
		1.38 (1.79)	2.00 (2.03)	3.05 (3.20)	6.61 (7.20)	7.79 (7.92)	
		–	1.86 (1.46)	0.87 (1.01)	5.26 (5.82)	3.99 (4.18)	
SAFT-VR Mie		1.75 (2.00)	1.59 (1.62)	2.07 (2.15)	10.95 (11.42)	14.96 (15.20)	
		1.75 (2.00)	2.06 (2.10)	3.92 (4.01)	11.72 (12.25)	16.92 (17.21)	
		–	1.41 (1.43)	1.19 (1.25)	10.13 (10.54)	12.87 (13.06)	
polar soft-SAFT		2.34 (2.41)	2.58 (3.09)	4.56 (4.56)	15.10 (14.95)	12.83 (12.77)	
		2.34 (2.41)	3.68 (3.90)	8.88 (9.02)	18.69 (18.39)	16.13 (16.00)	
		–	2.14 (2.76)	2.49 (2.45)	11.26 (11.29)	9.31 (9.33)	
BACKONE		3.97 (3.53)	2.20 (2.80)	2.20 (2.65)	11.69 (10.18)	6.18 (5.42)	
		3.97 (3.53)	4.30 (3.73)	4.34 (5.45)	12.06 (10.05)	6.62 (5.54)	
		–	1.36 (2.43)	1.18 (1.33)	11.28 (10.31)	5.70 (5.29)	
sCPA		1.78 (1.70)	1.76 (2.02)	2.52 (2.64)	10.41 (10.87)	11.45 (11.56)	
		1.78 (1.70)	2.49 (2.42)	5.00 (5.25)	11.15 (11.80)	9.53 (9.68)	
		–	1.47 (1.87)	1.34 (1.39)	9.62 (9.87)	13.50 (13.57)	
GERG-2008		0.56 (2.59)	1.31 (1.36)	2.25 (1.42)	3.56 (3.27)	0.41 (0.72)	
		0.56 (2.59)	1.90 (2.05)	4.78 (2.78)	3.45 (2.96)	0.48 (0.84)	
		–	1.08 (1.08)	1.04 (0.77)	3.67 (3.60)	0.34 (0.60)	
EOS-CG		0.56 (0.67)	1.31 (1.34)	2.26 (1.37)	3.32 (4.04)	0.63 (0.67)	
		0.56 (0.67)	1.90 (2.01)	4.79 (2.70)	3.34 (3.85)	0.60 (1.04)	
		–	1.08 (1.07)	1.05 (0.74)	3.30 (4.25)	0.66 (0.28)	

Results from predictions based on pure component models are compared to results that were obtained after adjusting binary parameters (given in brackets) to the training data. Results for δ^{rel} are reported for each EOS from top to bottom for all data, the training data, and the test data. For details, see text

A detailed discussion is given in the Supplementary Information. The speed of sound w is the only studied quantity, where the rotational and vibrational degrees of freedom, included in the ideal gas term \tilde{a}_{id} , cf. Eq. 1, influence the results. The GERG-2008 EOS yields the lowest deviations $\leq 0.5\%$ followed by the (simplified) EOS-CG with deviations $\leq 0.7\%$. From the remaining studied EOS, the PC-SAFT EOS yields the lowest deviations for the speed of sound $\leq 5\%$.

The results obtained from the adjusted models provide further interesting insights. While in most cases, significant improvements were observed for the modeling of the VLE phase behavior by adjusting binary interaction parameters (cf. Table 8 and Fig. 2), a more ambivalent picture evolves for the homogeneous state properties (cf. Table 9). In some cases, significant improvements are observed, e.g. for the adjusted GERG-2008 EOS for modeling the isothermal compressibility β as well as for the PC-SAFT EOS for most properties. Yet, in several cases, the model accuracy slightly decreases using an adjusted binary mixture parameter. This is likely due to the fact, that the description of the phase equilibrium and homogeneous state properties are conflicting objectives. Accordingly, improvements in the description of the phase equilibrium are bought at the expense of the decreasing accuracy for the modeling of the homogeneous state properties. This is particularly prominent for liquid state densities and speed of sound described by the adjusted GERG-2008 EOS and for the 2nd-order derivatives β and w described by the PCP-SAFT EOS. The EOS-CG yields slightly higher deviations for the liquid state densities and isothermal compressibility but lower deviations for the vapor state densities compared to the corresponding predictive mode results. For other properties and EOS, this conflicting objectives effect is also present, but less prominent. Overall, the EOS-CG and adjusted GERG-2008 yield the lowest deviations in the adjusted mode for homogeneous state properties. Also, the adjusted PCP-SAFT and PC-SAFT EOS yield a reasonably accurate description of the homogeneous state properties—in many cases well competitive to the multi-parameter EOS.

The deviations for the test data are in most cases lower compared to the deviations for the training data, cf. Table 9. This is likely due to the fact, that the data in the vicinity of the critical point of CO_2 is only included in the training data. Modeling this data is a challenging task for EOS and therefore yields larger deviations compared to the remaining data.

In most cases, the adjusted mode results for the test data show the same trend compared to the adjusted mode results for the training data. A lower deviation δ^{rel} for a given property in the training dataset leads to a lower deviation for this property in the test dataset, when compared to the predictive mode results. The adjusted parameters can, therefore, also be used to extrapolate to lower (or higher) temperatures and pressures for all studied EOS. Yet, these extrapolations should be done with caution.

4 Conclusions

Accurate models for the thermodynamic properties of the mixture $\text{CO}_2 + \text{O}_2$ are crucial for designing Allam cycle processes. In this work, different EOS were used for modeling the mixture $\text{CO}_2 + \text{O}_2$. First, the available literature data were critically reviewed and compiled in a database, which is provided in the electronic Supplementary Information. Two modeling approaches were used: (i) the EOS were used in a purely predictive mode and (ii) in an adjusted mode by parametrizing binary interaction parameters to experimental mixture data. In total, ten EOS were studied: two cubic [15, 16], six molecular-based [18, 21–28], and two multi-parameter EOS [20, 29].

Using adjusted mixture parameters does not automatically result in an improvement in the accuracy of all considered properties due to the conflicting objects during the fit, i.e. correct phase envelope and homogeneous state property description. The phase equilibrium predictions of the GERG-2008 EOS (i.e. no mixture parameters adjusted) show significant deviations to the experimental phase equilibrium data. The regression of the binary interaction parameter reduces the deviations of the compositions of the coexisting phases obtained from the GERG-2008 EOS drastically. Yet, this goes in hand with a decrease of the accuracy for some homogeneous state properties. Also, using the adjusted GERG-2008 model for extrapolation to lower temperatures results in significant deviations for the phase envelope.

The classical cubic PR EOS yields low deviations for the phase equilibrium predictions for the adjusted mode, but comparably large deviations for homogeneous state properties. The molecular-based EOS models, on the other hand, are an attractive alternative to the multi-parameter EOS. They provide robust extrapolation capabilities, but yield slightly less accurate description of the thermodynamic properties. In particular, the PCP-SAFT and SAFT-VR Mie models considered in this work yield a good performance. In both cases (cubic and molecular-based EOS), the extrapolation by the temperature-dependent binary interaction parameter results in lower deviations for the phase envelope at low temperatures ($T \lesssim 240$ K) compared to the GERG-2008 EOS. The EOS-CG (where the binary interaction parameters were regressed using data from a wider temperature range [29]) yields overall the lowest deviations for the phase envelopes at $T \lesssim 240$ K. In this work, reliable models for describing the mixture behavior $\text{CO}_2 + \text{O}_2$ were developed and compared to the EOS-CG model that was adjusted to mixture data in the literature. In particular, the adjusted GERG-2008, the PCP-SAFT, and the SAFT-VR Mie EOS as well as the EOS-CG from the literature provide accurate models for the thermodynamic properties of the mixture $\text{CO}_2 + \text{O}_2$. For future work, it would be interesting to apply these thermodynamic models for describing the actual Allam cycle in an exemplaric use case. Also, for a future work, testing the effects of more advanced mixing rules for the different EOS would be interesting.

The working fluid in the Allam cycle primarily consists of $\text{CO}_2 + \text{O}_2$. Yet, to some extent also water, nitrogen, argon, and other residue components are present in the process [3]. Extending the models to include these components in the parametrization and studying the influence of the obtained models on the description of the Allam cycle would be interesting.

5 Supplementary Information

Supplementary data can be found at <https://doi.org/10.1007/s10765-023-03297-w>. The numerical values for the experimental data for the $\text{CO}_2 + \text{O}_2$ mixture, cf. Tables 1 and 2, are reported as an electronic spreadsheet. The pure component parameters for CO_2 and O_2 for the studied EOS are reported. Furthermore, results for the phase envelope of temperatures below $T < 273$ K predicted and calculated by the studied EOS from this work are reported. Furthermore, the overestimation of

the critical point by molecular-based EOS and the poor description of the 2nd-order derivatives by the cubic and molecular-based EOS is discussed.

Supplementary Information The online version contains supplementary material available at <https://doi.org/10.1007/s10765-023-03297-w>.

Author Contributions JS: Data curation, formal analysis, methodology (equal), visualization, writing/original draft. GS: Writing/review and editing (supporting), validation (equal). SM: Writing/review and editing (supporting), validation (equal). HH: funding (equal), writing/review and editing (equal). SiSt: Funding (equal), conceptualization, supervision, methodology (equal), writing/review and editing (equal).

Funding Open Access funding enabled and organized by Projekt DEAL. S. Stephan gratefully acknowledges financial support of the present work by the IRTG 2057 (252408385).

Data Availability All literature data of the mixture $\text{CO}_2 + \text{O}_2$ used in this work are provided in the electronic Supplementary Information in a spreadsheet file. An explanation of that data are furthermore given in the Supplementary Information PDF file that can be found here <https://doi.org/10.1007/s10765-023-03297-w>.

Declarations

Competing interests The authors have no competing interests to declare that are relevant to the content of this article.

Open Access This article is licensed under a Creative Commons Attribution 4.0 International License, which permits use, sharing, adaptation, distribution and reproduction in any medium or format, as long as you give appropriate credit to the original author(s) and the source, provide a link to the Creative Commons licence, and indicate if changes were made. The images or other third party material in this article are included in the article's Creative Commons licence, unless indicated otherwise in a credit line to the material. If material is not included in the article's Creative Commons licence and your intended use is not permitted by statutory regulation or exceeds the permitted use, you will need to obtain permission directly from the copyright holder. To view a copy of this licence, visit <http://creativecommons.org/licenses/by/4.0/>.

References

1. R.J. Allam, M. Palmer, C. Hill, G.W. Brown, Jr., System and method for high efficiency power generation using a carbon dioxide circulating working fluid. Palmer Labs, LLC, assignee. Patent 2011/0179799, 31 August 2010 (2011)
2. R.J. Allam, M.R. Palmer, G.W. Brown, J. Fetvedt, D. Freed, H. Nomoto, M. Itoh, N. Okita, C. Jones, High efficiency and low cost of electricity generation from fossil fuels while eliminating atmospheric emissions. Including carbon dioxide. *Energy Procedia* **37**, 1135–1149 (2013). <https://doi.org/10.1016/j.egypro.2013.05.211>
3. R. Allam, S. Martin, B. Forrest, J. Fetvedt, X. Lu, D. Freed, G.W. Brown, T. Sasaki, M. Itoh, J. Manning, Demonstration of the Allam cycle: an update on the development status of a high efficiency supercritical carbon dioxide power process employing full carbon capture. *Energy Procedia* **114**, 5948–5966 (2017). <https://doi.org/10.1016/j.egypro.2017.03.1731>
4. S. Lasala, P. Chiesa, R. Privat, J.-N. Jaubert, VLE properties of CO_2 -based binary systems containing N_2 , O_2 and Ar: experimental measurements and modelling results with advanced cubic equations of state. *Fluid Phase Equilib.* **428**, 18–31 (2016). <https://doi.org/10.1016/j.fluid.2016.05.015>
5. S. Lasala, Advanced cubic equations of state for accurate modelling of fluid mixtures. application to CO_2 capture systems. PhD thesis, Politecnico di Milano Milan, Italy (2016). <https://doi.org/10.13140/RG.2.1.2948.9041>

6. S.F. Westman, H.G.J. Stang, S.W. Løvseth, A. Austegard, I. Snustad, I.S. Ertesvåg, Vapor–liquid equilibrium data for the carbon dioxide and oxygen ($\text{CO}_2 + \text{O}_2$) system at the temperatures 218, 233, 253, 273, 288 and 298 K and pressures up to 14 MPa. *Fluid Phase Equilib.* **421**, 67–87 (2016). <https://doi.org/10.1016/j.fluid.2016.04.002>
7. D. Lozano-Martín, G.U. Akubue, A. Moreau, D. Tuma, C.R. Chamorro, Accurate experimental (p , ρ , T) data of the ($\text{CO}_2 + \text{O}_2$) binary system for the development of models for CCS processes. *J. Chem. Thermodyn.* **150**, 106210 (2020). <https://doi.org/10.1016/j.jct.2020.106210>
8. D. Lozano-Martín, D. Vega-Maza, M.C. Martín, D. Tuma, C.R. Chamorro, Thermodynamic characterization of the ($\text{CO}_2 + \text{O}_2$) binary system for the development of models for CCS processes: Accurate experimental (p , ρ , T) data and virial coefficients. *J. Supercrit. Fluids* **169**, 105074 (2021). <https://doi.org/10.1016/j.supflu.2020.105074>
9. J.A. Commodore, C.E. Deering, R.A. Marriott, Volumetric properties and phase behavior of sulfur dioxide, carbon disulfide and oxygen in high-pressure carbon dioxide fluid. *Fluid Phase Equilib.* **477**, 30–39 (2018). <https://doi.org/10.1016/j.fluid.2018.08.012>
10. S. Ahamada, A. Valtz, S. Chabab, L. Blanco-Martín, C. Coquelet, Experimental density data of three carbon dioxide and oxygen binary mixtures at temperatures from 276 to 416 K and at pressures up to 20 MPa. *J. Chem. Eng. Data* **65**, 5313–5327 (2020). <https://doi.org/10.1021/acs.jced.0c00484>
11. N.I. Diamantonis, G.C. Boulougouris, E. Mansoor, D.M. Tsangaris, I.G. Economou, Evaluation of cubic, SAFT, and PC-SAFT equations of state for the vapor–liquid equilibrium modeling of CO_2 mixtures with other gases. *Ind. Eng. Chem. Res.* **52**, 3933–3942 (2013). <https://doi.org/10.1021/ie303248q>
12. M. Mazzoccoli, B. Bosio, E. Arato, S. Brandani, Comparison of equations-of-state with p – ρ – T experimental data of binary mixtures rich in CO_2 under the conditions of pipeline transport. *J. Supercrit. Fluids* **95**, 474–490 (2014). <https://doi.org/10.1016/j.supflu.2014.09.047>
13. A.G. Perez, C. Coquelet, P. Paricaud, A. Chapoy, Comparative study of vapour–liquid equilibrium and density modelling of mixtures related to carbon capture and storage with the SRK, PR, PC-SAFT and SAFT-VR Mie equations of state for industrial uses. *Fluid Phase Equilib.* **440**, 19–35 (2017). <https://doi.org/10.1016/j.fluid.2017.02.018>
14. O. Redlich, J.N.S. Kwong, On the thermodynamics of solutions. V. An equation of state. Fugacities of gaseous solutions. *Chem. Rev.* **44**, 233–244 (1949). <https://doi.org/10.1021/cr60137a013>
15. G. Soave, Equilibrium constants from a modified Redlich–Kwong equation of state. *Chem. Eng. Sci.* **27**, 1197–1203 (1972). [https://doi.org/10.1016/0009-2509\(72\)80096-4](https://doi.org/10.1016/0009-2509(72)80096-4)
16. D.-Y. Peng, D.B. Robinson, A new two-constant equation of state. *Ind. Eng. Chem. Fundam.* **15**, 59–64 (1976). <https://doi.org/10.1021/i160057a011>
17. W.G. Chapman, K.E. Gubbins, G. Jackson, M. Radosz, SAFT: equation-of-state solution model for associating fluids. *Fluid Phase Equilib.* **52**, 31–38 (1989). [https://doi.org/10.1016/0378-3812\(89\)80308-5](https://doi.org/10.1016/0378-3812(89)80308-5)
18. J. Gross, G. Sadowski, Perturbed-chain SAFT: an equation of state based on a perturbation theory for chain molecules. *Ind. Eng. Chem. Res.* **40**, 1244 (2001). <https://doi.org/10.1021/ie0003887>
19. K.E. Starling, M.S. Han, Thermo data refined for LPG, part 14: mixtures. *Hydrocarb. Process.* **51**, 129–132 (1972)
20. O. Kunz, W. Wagner, The GERG-2008 wide-range equation of state for natural gases and other mixtures: an expansion of GERG-2004. *J. Chem. Eng. Data* **57**, 3032–3091 (2012). <https://doi.org/10.1021/je300655b>
21. T. Lafitte, A. Apostolalou, C. Avendaño, A. Galindo, C.S. Adjiman, E.A. Müller, G. Jackson, Accurate statistical associating fluid theory for chain molecules formed from Mie segments. *J. Chem. Phys.* **139**, 154504 (2013). <https://doi.org/10.1063/1.4819786>
22. J. Gross, An equation-of-state contribution for polar components: quadrupolar molecules. *AIChE J.* **51**, 2556–2568 (2005). <https://doi.org/10.1002/aic.10502>
23. F.J. Blas, L.F. Vega, Thermodynamic behaviour of homonuclear and heteronuclear Lennard–Jones chains with association sites from simulation and theory. *Mol. Phys.* **92**, 135–150 (1997). <https://doi.org/10.1080/002689797170707>
24. I.I.I. Alkhatib, L.M.C. Pereira, J. Torne, L.F. Vega, Polar soft-SAFT: theory and comparison with molecular simulations and experimental data of pure polar fluids. *Phys. Chem. Chem. Phys.* **22**, 13171–13191 (2020). <https://doi.org/10.1039/D0CP00846J>
25. A. Müller, J. Winkelmann, J. Fischer, Backbone family of equations of state: 1. Nonpolar and polar pure fluids. *AIChE J.* **42**, 1116–1126 (1996). <https://doi.org/10.1002/aic.690420423>

26. U. Weingerl, M. Wendland, J. Fischer, A. Müller, J. Winkelmann, Backbone family of equations of state: 2. nonpolar and polar fluid mixtures. *AIChE J.* **47**, 705–717 (2001). <https://doi.org/10.1002/aic.690470317>
27. G.M. Kontogeorgis, I.V. Yakoumis, H. Meijer, E. Hendriks, T. Moorwood, Multicomponent phase equilibrium calculations for water–methanol–alkane mixtures, *Fluid Phase Equilib.* **158–160**, 201–209 (1999). [https://doi.org/10.1016/S0378-3812\(99\)00060-6](https://doi.org/10.1016/S0378-3812(99)00060-6)
28. G.M. Kontogeorgis, M.L. Michelsen, G.K. Folas, S. Derawi, N. Solms, E.H. Stenby, Ten years with the CPA (cubic-plus-association) equation of state. Part I. Pure compounds and self-associating systems. *Ind. Eng. Chem. Res.* **45**, 4855–4868 (2006). <https://doi.org/10.1021/ie051305v>
29. J. Gernert, R. Span, EOS-CG: a Helmholtz energy mixture model for humid gases and CCS mixtures. *J. Chem. Thermodyn.* **93**, 274–293 (2016). <https://doi.org/10.1016/j.jct.2015.05.015>
30. R. Span, W. Wagner, A new equation of state for carbon dioxide covering the fluid region from the triple-point temperature to 1100 K at pressures up to 800 MPa. *J. Phys. Chem. Ref. Data* **25**, 1509–1596 (1996). <https://doi.org/10.1063/1.555991>
31. R. Span, W. Wagner, Equations of state for technical applications. II. results for nonpolar fluids. *Int. J. Thermophys.* **24**, 41–109 (2003). <https://doi.org/10.1023/A:1022310214958>
32. S. Angus, B. Armstrong, R.B. Reuck, *International Thermodynamic Tables of the Fluid State-3 Carbon Dioxide* (Pergamon, New York, 1976)
33. P.J. Linstrom, W.G. Mallard, NIST Chemistry WebBook, NIST Standard Reference Database Number 69. National Institute of Standards and Technology, Gaithersburg (retrieved June 2023) (2023). <https://doi.org/10.18434/T4D303>
34. M. Mantovani, P. Chiesa, G. Valenti, M. Gatti, S. Consonni, Supercritical pressure–density–temperature measurements on CO₂–N₂, CO₂–O₂ and CO₂–Ar binary mixtures. *J. Supercrit. Fluids* **61**, 34–43 (2012). <https://doi.org/10.1016/j.supflu.2011.09.001>
35. P.H. Konyonenburg, R.L. Scott, Critical lines and phase equilibria in binary van der Waals mixtures. *Philos. Trans. R. Soc. Lond.* **298**, 495–540 (1980). <https://doi.org/10.1098/rsta.1980.0266>
36. A.M.A. Dias, J.C. Pàmies, Ja.A.P. Coutinho, I.M. Marrucho, L.F. Vega, SAFT modeling of the solubility of gases in perfluoroalkanes. *J. Phys. Chem. B* **108**, 1450–1457 (2004). <https://doi.org/10.1021/jp036225o>
37. I.I.I. Alkhatib, F. Llovel, L.F. Vega, Assessing the effect of impurities on the thermophysical properties of methane-based energy systems using polar soft-SAFT. *Fluid Phase Equilib.* **527**, 112841 (2021). <https://doi.org/10.1016/j.fluid.2020.112841>
38. S. Dufal, T. Lafitte, A. Galindo, G. Jackson, A.J. Haslam, Developing intermolecular-potential models for use with the SAFT-VR Mie equation of state. *AIChE J.* **61**, 2891–2912 (2015). <https://doi.org/10.1002/aic.14808>
39. N.I. Diamantonis, I.G. Economou, Evaluation of statistical associating fluid theory (SAFT) and perturbed chain-SAFT equations of state for the calculation of thermodynamic derivative properties of fluids related to carbon capture and sequestration. *Energy Fuels* **25**, 3334–3343 (2011). <https://doi.org/10.1021/ef200387p>
40. I. Tsivintzelis, G.M. Kontogeorgis, M.L. Michelsen, E.H. Stenby, Modeling phase equilibria for acid gas mixtures using the CPA equation of state. Part II: binary mixtures with CO₂. *Fluid Phase Equilib.* **306**, 38–56 (2011). <https://doi.org/10.1016/j.fluid.2011.02.006>
41. L. Sun, X. Liang, N. Solms, G.M. Kontogeorgis, Solubility modeling of air in aqueous electrolyte solutions with the e-CPA equation of state. *Ind. Eng. Chem. Res.* **59**, 18693–18704 (2020). <https://doi.org/10.1021/acs.iecr.0c03164>
42. R. Klimeck, Entwicklung einer Fundamentalgleichung für Erdgase für das Gas- und Flüssigkeitsgebiet sowie das Phasengleichgewicht. PhD thesis, Fakultät für Maschinenbau, Ruhr-Universität Bochum, Bochum (2000)
43. R. Schmidt, W. Wagner, A new form of the equation of state for pure substances and its application to oxygen. *Fluid Phase Equilib.* **19**, 175–200 (1985). [https://doi.org/10.1016/0378-3812\(85\)87016-3](https://doi.org/10.1016/0378-3812(85)87016-3)
44. R. Span, W. Wagner, Equations of state for technical applications. I. Simultaneously optimized functional forms for nonpolar and polar fluids. *Int. J. Thermophys.* **24**, 1–39 (2003). <https://doi.org/10.1023/A:1022390430888>
45. R. Span, W. Wagner, On the extrapolation behavior of empirical equations of state. *Int. J. Thermophys.* **18**, 1415–1443 (1997). <https://doi.org/10.1007/BF02575343>
46. S. Stephan, U.K. Deiters, Characteristic curves of the Lennard–Jones fluid. *Int. J. Thermophys.* **41**, 147 (2020). <https://doi.org/10.1007/s10765-020-02721-9>

47. J. Staubach, S. Stephan, Prediction of thermodynamic properties of fluids at extreme conditions: assessment of the consistency of molecular-based models. In: Aurich, J.C., Garth, C., Linke, B.S. (eds.) Proceedings of the 3rd Conference on Physical Modeling for Virtual Manufacturing Systems and Processes, pp. 170–188 (2023). https://doi.org/10.1007/978-3-031-35779-4_10
48. R. Span, Multiparameter Equations of State. Springer, Berlin (2000). <https://doi.org/10.1007/978-3-662-04092-8>
49. E.W. Lemmon, R.T. Jacobsen, A generalized model for the thermodynamic properties of mixtures. *Int. J. Thermophys.* **20**, 825–835 (1999). <https://doi.org/10.1023/A:1022627001338>
50. I.H. Bell, A. Jäger, Helmholtz energy transformations of common cubic equations of state for use with pure fluids and mixtures. *J. Res. Natl. Inst. Stand. Technol.* **121**, 238–263 (2016). <https://doi.org/10.6028/jres.121.011>
51. G. Mie, Zur kinetischen Theorie der einatomigen Körper. *Ann. Phys.* **316**, 657–697 (1903). <https://doi.org/10.1002/andp.19033160802>
52. E. Schäfer, G. Sadowski, S. Enders, Interfacial tension of binary mixtures exhibiting azeotropic behavior: measurement and modeling with PCP-SAFT combined with density gradient theory. *Fluid Phase Equilib.* **362**, 151 (2014). <https://doi.org/10.1016/j.fluid.2013.09.042>
53. N. Solms, M.L. Michelsen, G.M. Kontogeorgis, Prediction and correlation of high-pressure gas solubility in polymers with simplified PC-SAFT. *Ind. Eng. Chem. Res.* **44**, 3330–3335 (2005). <https://doi.org/10.1021/ie049089y>
54. M. Yarrison, W.G. Chapman, A systematic study of methanol+n-alkane vapor–liquid and liquid–liquid equilibria using the CK-SAFT and PC-SAFT equations of state. *Fluid Phase Equilib.* **226**, 195–205 (2004). <https://doi.org/10.1016/j.fluid.2004.09.024>
55. I. Antolović, J. Staubach, S. Stephan, J. Vrabec, Phase equilibria of symmetric Lennard–Jones mixtures and a look at the transport properties near the upper critical solution temperature. *Phys. Chem. Chem. Phys.* **25**, 17627–17638 (2023). <https://doi.org/10.1039/D3CP01434G>
56. F. Llovel, C.J. Peters, L.F. Vega, Second-order thermodynamic derivative properties of selected mixtures by the soft-SAFT equation of state. *Fluid Phase Equilib.* **248**, 115–122 (2006). <https://doi.org/10.1016/j.fluid.2006.07.018>
57. X. Liang, K. Thomsen, W. Yan, G.M. Kontogeorgis, Prediction of the vapor–liquid equilibria and speed of sound in binary systems of 1-alkanols and n-alkanes with the simplified PC-SAFT equation of state. *Fluid Phase Equilib.* **360**, 222–232 (2013). <https://doi.org/10.1016/j.fluid.2013.09.037>
58. M. Khammar, J.M. Shaw, Speed of sound prediction in 1-n-alcohol+n-alkane mixtures using a translated SAFT-VR-Mie equation of state. *Fluid Phase Equilib.* **288**, 145–154 (2010). <https://doi.org/10.1016/j.fluid.2009.10.022>
59. S. Stephan, J. Staubach, H. Hasse, Review and comparison of equations of state for the Lennard–Jones fluid. *Fluid Phase Equilib.* **523**, 112772 (2020). <https://doi.org/10.1016/j.fluid.2020.112772>
60. J. Gross, G. Sadowski, Application of the perturbed-chain SAFT equation of state to associating systems. *Ind. Eng. Chem. Res.* **41**, 5510–5515 (2002). <https://doi.org/10.1021/ie010954d>
61. M. Ahmad, J. Gernert, E. Wilbers, Effect of impurities in captured CO₂ on liquid–vapor equilibrium. *Fluid Phase Equilib.* **363**, 149–155 (2014). <https://doi.org/10.1016/j.fluid.2013.11.009>
62. A. Fredenslund, M. Jørgen, O. Persson, Gas–liquid equilibrium of oxygen–carbon dioxide system. *J. Chem. Eng. Data* **17**, 440–443 (1972). <https://doi.org/10.1021/je60055a019>
63. A. Fredenslund, G. Sather, Gas–liquid equilibrium of the oxygen–carbon dioxide system. *J. Chem. Eng. Data* **15**, 17–22 (1970). <https://doi.org/10.1021/je60044a024>
64. G.-I. Kaminishi, T. Toriumi, Gas–liquid equilibrium under high pressures. VI. Vapor–liquid phase equilibrium in the CO₂-H₂, CO₂-N₂, and CO₂-O₂ systems. *J. Soc. Chem. Ind. Jpn.* **69**, 175–178 (1966). https://doi.org/10.1246/nikkashi1898.69.2_175
65. P.L. Chueh, N.K. Muirbrook, J.M. Prausnitz, Multicomponent vapor–liquid equilibria at high pressures: Part II. Thermodynamic analysis. *AIChE J.* **11**, 1097–1102 (1965). <https://doi.org/10.1002/aic.690110625>
66. G.H. Zenner, L.I. Dana, Liquid–vapor equilibrium compositions of carbon dioxide–oxygen–nitrogen mixtures. *Chem. Eng. Prog. Symp. Ser.* **44**, 36–41 (1963)
67. I. Al-Siyabi, Effect of impurities on CO₂ stream properties. PhD thesis, Heriot-Watt University (2013). <http://hdl.handle.net/10399/2643>
68. M. Mazzocoli, B. Bosio, E. Arato, Pressure–density–temperature measurements of binary mixtures rich in CO₂ for pipeline transportation in the CCS process. *J. Chem. Eng. Data* **57**, 2774–2783 (2012). <https://doi.org/10.1021/je300590v>

69. G.J. Gururaja, M.A. Tirunarayanan, A. Ramachandran, Dynamic viscosity of gas mixtures. *J. Chem. Eng. Data* **12**, 562–567 (1967). <https://doi.org/10.1021/je60035a024>

Publisher's Note Springer Nature remains neutral with regard to jurisdictional claims in published maps and institutional affiliations.